JOURNAL OF GEOPHYSICAL RESEARCH, VOL. 113, A07305, doi:10.1029/2007JA012897, 2008

Ionospheric annual asymmetry observed by the COSMIC radio occultation measurements and simulated by the TIEGCM

Zhen Zeng,[1,2] Alan Burns,[1] Wenbin Wang,[1] Jiuhou Lei,[1] Stan Solomon,[1] Stig Syndergaard,[2] Liying Qian,[1] and Ying-Hwa Kuo[2]

Received 18 October 2007; revised 26 December 2007; accepted 5 February 2008; published 11 July 2008.

[1] Average F_2-layer electron densities at December solstice are higher than those at June solstice. This phenomenon, which is often called the F_2-layer annual asymmetry, has been observed for several decades, but its causes are still not fully understood. This study investigates global variations of this annual asymmetry observed from one year of the Constellation Observing System for Meteorology, Ionosphere and Climate (COSMIC) ionospheric radio occultation (IRO) measurements. The IRO observations show that there is a strong NmF2 annual asymmetry that has significant longitudinal and local time variations. A strong peak of the asymmetry occurs at about noon and another one at midnight, both located at around 25° geomagnetic latitude. Numerical simulations using the Thermosphere-Ionosphere Electrodynamics Global Circulation Model (TIEGCM) are in very good agreement with these observations. The modeled NmF2 annual asymmetry has a similar magnitude, and similar semidiurnal and longitudinal variations as those in the observations. TIEGCM simulations show that changes in solar extreme ultraviolet (EUV) radiation between the December and June solstices and the displacement of the geomagnetic axis from the geographic axis are the two primary processes that cause the annual asymmetry and its associated longitudinal and local time variations. The tides propagating from lower altitudes also contribute to this asymmetry, but to a smaller extent.

Citation: Zeng, Z., A. Burns, W. Wang, J. Lei, S. Solomon, S. Syndergaard, L. Qian, and Y.-H. Kuo (2008), Ionospheric annual asymmetry observed by the COSMIC radio occultation measurements and simulated by the TIEGCM, *J. Geophys. Res.*, *113*, A07305, doi:10.1029/2007JA012897.

1. Introduction

[2] The ionosphere is a region of the Earth's atmosphere in which the plasma densities are sufficiently high to affect the dynamical behavior of both the ionized and neutral gases, as well as the propagation of radio waves. It is formed mainly by photoionization of the neutral gases by extreme ultraviolet (EUV) radiation from the sun. The production rate of the electrons is proportional to the neutral gas density and solar radiation intensity. In the lower ionosphere (D, E, and F_1-layers) photochemical equilibrium is achieved and electron densities are determined primarily by the balance between photoionization production and chemical loss. At higher altitudes in the F_2-layer, chemical loss becomes less important since neutral densities decrease exponentially with height. Thus the lifetime of the ions become sufficiently long so that plasma transport processes, such as ambipolar diffusion and plasma drift caused by electric fields, contribute significantly to the global structure and dynamical behavior of the ionospheric F_2-layer [*Kelley and Heelis*, 1989]. The ionosphere changes with geophysical conditions, and exhibits significant diurnal, seasonal, and solar cycle variations. In addition, the ionospheric F_2-layer can behave abnormally in its global structures and temporal variations. These anomalies include the equatorial anomaly, the winter anomaly, the semiannual anomaly and the annual asymmetry [e.g., *Rishbeth*, 1998]. In this paper, we will investigate the ionospheric annual asymmetry, which is characterized by the electron density being 30% larger near the December solstice than it is near the June solstice on global average. This asymmetry has been observed for decades, but its mechanism has not been fully understood. Explaining the annual asymmetry has been listed as one of the top scientific targets in ionospheric studies [*Rishbeth*, 2007].

[3] The annual asymmetry was first reported in 1930s [*Berkner and Wells*, 1938] and has been further studied using the NmF2 data from pairing ionosonde measurements [*Yonezawa*, 1971; *Rishbeth and Müller-Wodarg*, 2006], the total electron content (TEC) data from a worldwide network of global positioning system (GPS) observations [*Mendillo et al.*, 2005], and topside ionospheric observations [*Su et al.*, 1998; *Liu et al.*, 2007]. These studies show that the asymmetry is strong at noon and at midnight, occurring at

[1] High Altitude Observatory, National Center for Atmospheric Research, Boulder, Colorado, USA.
[2] COSMIC Project Office, University Corporation for Atmospheric Research, Boulder, Colorado, USA.

0148-0227/08/2007JA012897$09.00

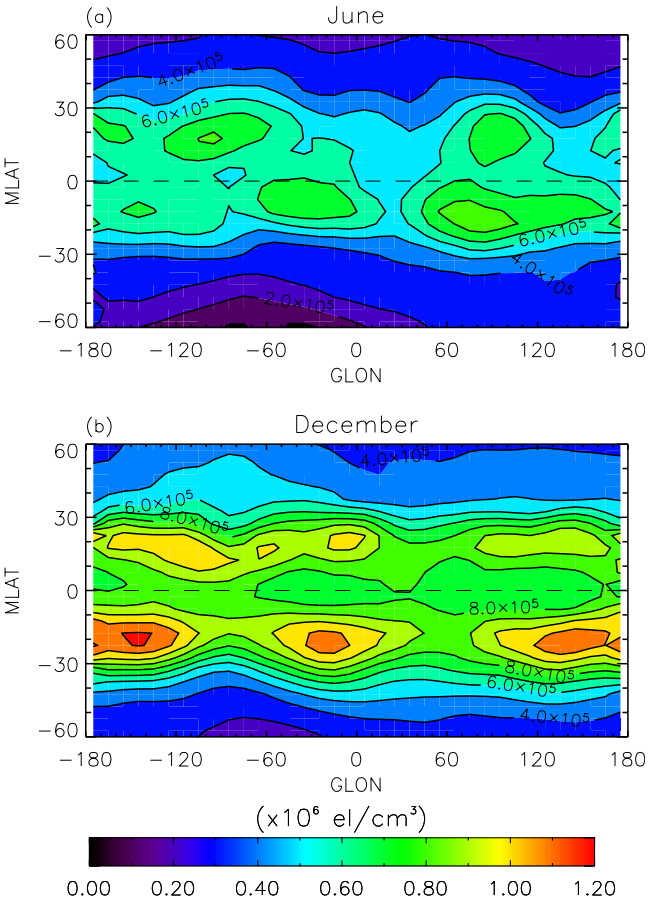

Figure 1. Global NmF2 maps at noon derived from COSMIC IRO measurements for (a) June and (b) December solstices in geographic longitude (GLON) and geomagnetic latitude (MLAT) coordinates. The color contours give the values of NmF2 with a contour interval of 1×10^5 el/cm^3.

all latitudes from equatorial to subauroral regions, and tends to be greater at solar minimum than solar maximum. *Rishbeth and Müller-Wodarg* [2006] used the Coupled Thermosphere-Ionosphere-Plasmasphere (CTIP) model to simulate the annual asymmetry. Their simulation results gave much smaller annual asymmetry in electron densities than was observed. Two possible mechanisms for the asymmetry: varying Sun-Earth distance (0.983 astronomical unit (AU) for December, 1.017 AU for June) and tides in the lower boundary of the CTIP model, were investigated, but the model failed to fully reproduce the observed asymmetry. They then speculated several possible causes of the annual asymmetry which are yet to be verified, such as other ionizing sources from different spectral bands of solar radiations than EUV or from extraterrestrial environment, the hemispheric asymmetry of the geomagnetic field, or other causes from the lower atmosphere other than tides.

[4] In this study, we use the NmF2 data retrieved from the COSMIC radio occultation (RO) measurements for studying the annual asymmetry. COSMIC is a collaborative mission between United States and Taiwan, which launched six microsatellites into a circular, 72° inclination orbit at an altitude of 512 km on 15 April 2006. The GPS RO receiver aboard each COSMIC satellite tracks the radio signals from GPS satellites in limb view as they are occulted by the Earth's atmosphere. By measuring the phase change of the radio signal the vertical electron density profile can be obtained by numerical inversion [*Schreiner et al.*, 1999; *Lei et al.*, 2007]. The intercomparison among collocated IRO profiles during the first few months of the COSMIC mission [*Schreiner et al.*, 2007] and comparison of IRO profiles with those measured by Incoherent Scatter Radars and ionosondes [*Lei et al.*, 2007] show that electron density profiles retrieved from COSMIC IRO measurements are in good agreement with those from other observations. An obvious advantage of the COSMIC measurements as opposed to ground-based ionosondes and TEC observations is their global coverage and large amount of data (up to 3000 globally distributed profiles per day), which provides an opportunity to study global nature of the annual asymmetry.

[5] In section 2, we show the annual asymmetry observed by COSMIC using IRO data collected in 2006–2007 and we describe the method of quantifying the asymmetry. In section 3 we present the simulated annual asymmetry using the NCAR Thermosphere-Ionosphere Electrodynamics Global Circulation Model (TIEGCM), which agrees well with the observed one. We then examine the various mechanisms that might be responsible for the annual asymmetry using TIEGCM, and estimate their relative contributions by controlled simulation studies. Finally we summarize our findings in section 4.

2. COSMIC IRO Data and Annual Asymmetry

[6] The retrieved peak densities (NmF2) from the COSMIC measurements during a 91-day period that centered on 21 June and 21 December in 2006, representing the observations on the June and December solstices respectively, are used in this study. All data are downloaded from the website of the University Corporation for Atmospheric Research (UCAR) COSMIC Data Analysis and Archival Center (CDAAC) (http://www.cosmic.ucar.edu). All COSMIC observations under geomagnetic disturbed conditions with Kp index larger than 3 are removed. The solar activity was low during these two periods, with the averaged $F_{10.7}$ solar flux for the June and December solstices being 76.4 sfu and 82.2 sfu (1 sfu = 10^{-22} Wm^{-2} Hz^{-1}), respectively. The remaining data are divided into different subsets distributed in a uniform horizontal grid with a resolution of 10° in geographic longitude and 5° in geomagnetic latitude. For each subset, the data are sorted in local time (LT) and averaged [*Beers et al.*, 1990] within a 2 h sliding window with a 1 h moving step. Because the orbits of the COSMIC satellites were very close to each other in the first few months following launch, the COSMIC soundings were clustered in a limited local time slowly shifted day by day. Though 91-d periods help to increase the LT coverage as well as the occultation number on each grid, a seventh-order polynomial fitting was applied on the averaged data to cover the possible data gaps in the LT domain.

[7] Figure 1 shows global maps of NmF2 at noon as a function of geographic longitude (GLON) and geomagnetic latitude (MLAT) for the June (Figure 1a) and December (Figure 1b) solstices, respectively. The equatorial anomaly is clearly seen at both solstices, with crests in NmF2 located around ±20° MLAT. The equatorial anomaly also shows

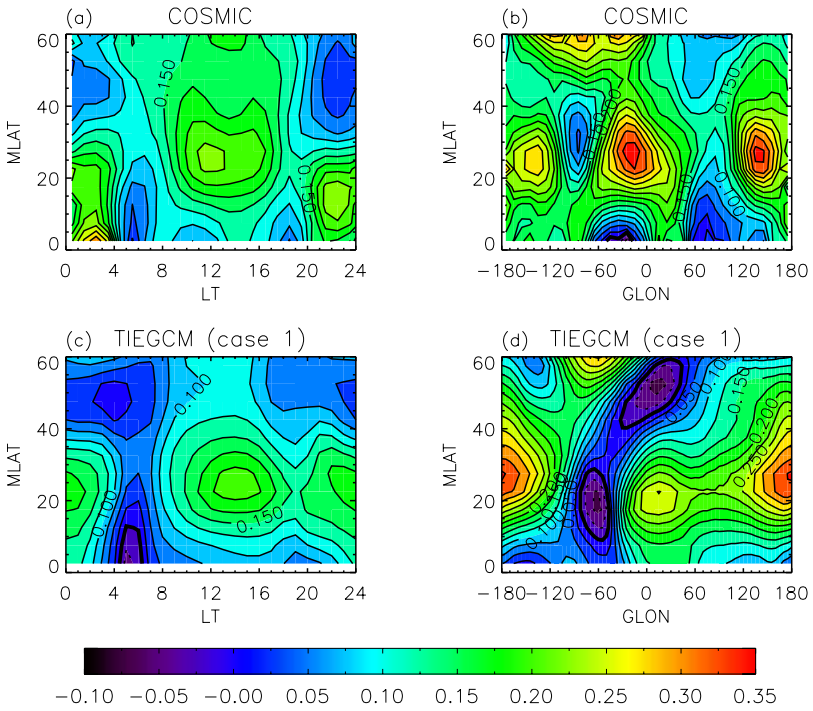

Figure 2. Local time (LT) variations of the zonal mean asymmetry index (AI) (left, contour interval: 0.025) and geographic longitudinal (GLON) variations of the noontime AI (right, contour interval: 0.025) for different geomagnetic latitudes (MLAT) calculated from the COSMIC IRO observations (upper) and TIEGCM simulations (lower).

significant longitudinal variations, which has been investigated in many studies through the displacement of geomagnetic and geographic equators, the magnetic declination angle at the magnetic equator, equatorial electric field and magnetic field, and nonmigrating tidal forcing from below [*Su et al.*, 1997; *Millward et al.*, 2001; *Sagawa et al.*, 2005]. The NmF2 values in the June solstice were around 30% smaller than those in the December solstice in both hemispheres. This clearly shows the annual asymmetry.

[8] In order to quantify the annual asymmetry we use the "asymmetry index" (AI), which was developed by *Rishbeth and Müller-Wodarg* [2006]. The AI is defined as

$$\mathrm{AI}(\theta,\ \lambda) = \frac{\mathrm{NmF2}_{\mathrm{NS\_Dec}}(\theta,\ \lambda) - \mathrm{NmF2}_{\mathrm{NS\_Jun}}(\theta, \lambda)}{\mathrm{NmF2}_{\mathrm{NS\_Dec}}(\theta,\ \lambda) + \mathrm{NmF2}_{\mathrm{NS\_Jun}}(\theta, \lambda)}, \quad (1)$$

where θ is the MLAT which runs from 0° at the equator and 90° at the pole, while λ is the GLON, $\mathrm{NmF2}_{\mathrm{NS}}$ $(\theta,\ \lambda) = 1/2$ $(\mathrm{NmF2}(\theta,\ \lambda) + \mathrm{NmF2}(-\theta,\ \lambda))$ with subscripts Dec, Jun denoting the December and June solstices, which represents the mean of northern and southern hemisphere values of NmF2. The AI is positive if NmF2 on the December solstice is larger than that on the June solstice, and negative if NmF2 is smaller on the December solstice than on the June solstice. For instance, an AI of 0.2 corresponds to a December/June ratio of $\mathrm{NmF2}_{\mathrm{NS}}$ equals to 1.5.

[9] Applying equation (1) to the NmF2 map from COSMIC IRO measurements in Figure 1 yield a global pattern of the annual asymmetry index. Figure 2a gives the LT variation of the longitudinally averaged AI for different magnetic latitudes. This LT variation has not been noted in previous studies. The zonal mean AI is globally positive, indicating that zonal mean electron densities are higher near the December solstice than they are near the Jun. solstice. The global mean AI is about 0.14, corresponding to ~30% departure from hemispheric symmetry. This value is close to those of the annual asymmetry from other data sources [*Mendillo et al.*, 2005; *Rishbeth and Müller-Wodarg*, 2006]. Two peaks occur at 25° MLAT near noon and at MLAT near 15° around midnight.

[10] To illustrate the longitudinal variations of the AI, Figure 2b show the AI map at noon as an example. The AI is still dominated by positive values, with a maximum of about 0.36. Three peaks of the AI occur at 140°W, 20°W, and 140°E near 25° MLAT, which yields a strong asymmetry at noontime as shown in Figure 2a. Additional structure is seen at latitudes above 50°, with a crest of the asymmetry in the western hemisphere merging into the low-latitude and a trough in the eastern hemisphere. Near the magnetic equator region (0°–15° in MLAT), the AI is low. Similar AI structure has also been shown by *Mendillo et al.* [2005], based on global TEC observations.

3. TIEGCM Simulation Results

3.1. TIEGCM Model

[11] The NCAR TIEGCM is a time dependent, three-dimensional model that solves the energy, momentum, and continuity equations of the coupled thermosphere/ionosphere self-consistently [*Richmond et al.*, 1992]. The horizontal grid of the model is 5° × 5° in latitude and longitude. There are 29 pressure surfaces extending from 97 km to about 700 km (depending on the solar activity) with a

Table 1. Basic Parameter Settings for Geomagnetic Field Configuration (Column 2), Sun-Earth Distance (Column 3), Tidal Forcing on the Lower Boundary (Column 4), and Corresponding Figure (Column 5) for Different Case (Column 1) Studies With the TIEGCM Model

Case	Magnetic Field Conf.	Sun-Earth Distance	Tides	Figures
1	IGRF	varying	√	Figures 2c and 2d
2	tilted dipole	varying	√	Figures 3 and 4a
3	aligned dipole	varying	√	Figures 3 and 4b
4	aligned dipole	fixed	√	Figures 3 and 4c
5	aligned dipole	fixed		Figures 3 and 4d
6	IGRF	fixed	√	Figure 5a
7	IGRF	fixed		Figure 5b

vertical resolution of half scale height. At the upper boundary, the vertical O^+ flux is specified, which approximates the plasma exchange between the plasmasphere and the ionosphere. The migrating diurnal and semidiurnal tidal perturbations calculated by the Global Scale Wave Model (GSWM) [*Hagan et al.*, 1999] are specified at the lower boundary to account for the dynamical coupling between the lower and middle atmosphere and the upper atmosphere. The representative capability of the GSWM has been diagnosed widely through comparative analyses with observational data and other models [*Manson et al.*, 1999; *Pancheva et al.*, 2002]. In the standard TIEGCM run, the geomagnetic field model is specified by the International Geomagnetic Reference Field (IGRF) 1995 (IGRF is a mathematical model of the Earth's main field and its secular variation, which comprises a set of spherical harmonic (or Gauss) coefficients, g_n^m and h_n^m, in a series expansion of the geomagnetic potential (please refer to http://www.ngdc.noaa.gov/IAGA/vmod/igrf.html). For the IGRF 1995 model, the first eight Gauss coefficients define an eccentric dipole, which is both offset and tilted with respect to the Earth's rotation axis; while the first three Gauss coefficients represent contributions to a centered tilted dipole.), using Magnetic Apex coordinates [*Richmond*, 1995b]. Input parameters for the TIEGCM include the solar flux $F_{10.7}$, the integrated hemispheric power of precipitating auroral electrons (HP) and the cross polar cap potential (CP). Throughout this study, HP = 16 GW and CP = 45 kV, which are typical values for geomagnetic quiet conditions.

3.2. Real-Case Simulation

[12] All the simulations focused on the northern (21 June) and southern (21 December) solstices under quiet geomagnetic conditions, corresponding to the COSMIC observations in Figure 1. F10.7 index, as a good proxy for solar radiation, was set to 80 for both solstices in all simulation, which was comparable to observed 91-day averages of F10.7 for June (76.4) and for December (82.2). Other parameter settings for different simulation cases are summarized in Table 1. In case 1, the geomagnetic field was specified by the IGRF model, and tidal forcing from the lower atmosphere was specified by the GSWM. The variation of the Sun-Earth distance was included in the model run. Case 1 is referred as the real case simulation, because observed F10.7 difference between solstices would approximately bring in 7% variation in solar radiation, which is comparable to those caused by the native variation of 3.5% in Sun-Earth distance.

[13] The annual asymmetry index AI was calculated from the simulated NmF2 using equation (1). Figure 2c illustrates the pattern of the zonal mean AI simulated by the model in LT and MLAT coordinates. The AI is almost all positive with a global mean of 0.11, which is comparable to the observed value. Strong asymmetries are mainly located at around 25° MLAT. A maximum is seen near 14 LT at 25° MLAT with a magnitude of around 0.23. Small values of AI are seen at 0°–15° MLAT near dawn, and at 40°–60° MLAT at night. The modeled daytime peak near 25° MLAT is slightly weaker in magnitude and two hours later in time than the noon peak in the observations (Figure 2a). Nevertheless, the TIEGCM simulations captured the overall pattern of the observed zonal mean asymmetry with roughly the same magnitudes. Both the model simulations and observations show significant local time and latitudinal variations of the AI, with strong asymmetry occurring near 25° MLAT, and a clear diurnal signature at magnetic latitudes over 40°.

[14] Figure 2d gives the noon AI simulated by the TIEGCM in geographic longitude and geomagnetic latitude. The strongest asymmetry in AI of 0.35 is seen at 180°E, and a secondary peak of AI occurs at 10°E near 20° MLAT. Another peak is seen at subauroral latitudes at 60°W. Weak asymmetry regions (blue shaded areas in Figure 2d) are located at 60°W at 25° MLAT and 0°E at 50° MLAT, respectively. When compared with the daytime AI pattern observed by COSMIC (Figure 2b), the AI structure from the TIEGCM simulations is similar, with maxima occurring near 25° and 60° MLAT, though the two separate maxima near ±150°E at 25° MLAT in Figure 2b are merged together in Figure 2d to form a single strong peak.

[15] In brief, the TIEGCM simulations reproduced many features of the observed annual asymmetry, both in magnitude and variation. This suggests that the TIEGCM can be used to investigate the physical mechanisms causing the annual asymmetry.

3.3. Case-Controlled Studies

[16] Three parameters were varied in our controlled case studies using the TIEGCM. These parameters are: the Sun-Earth distance, the geomagnetic field configuration, and the inclusion of lower atmospheric tides. Solar EUV radiation is the main source of ionization at low and middle latitudes under quiet geomagnetic conditions. Changes in solar EUV radiation by the varying Sun-Earth distance between June and December solstices, may cause parts of the ionospheric annual asymmetry. A hypothetical change in the geomagnetic configuration (e.g., if the geomagnetic poles were not displaced from the geographic poles), can alter the coupling between the neutral wind circulation and the ionospheric electrodynamics. Thus the geomagnetic field configuration may also be partly responsible for the asymmetric electron density distributions. Upwardly propagating tides from the lower atmosphere, the main driver of the daytime dynamo field, may also contribute to the annual asymmetry.

[17] To understand which of, and to what degree these physical mechanisms are responsible for the F_2-layer annual asymmetry, six controlled numerical experiments were performed. The parameter settings are listed as cases 2–7

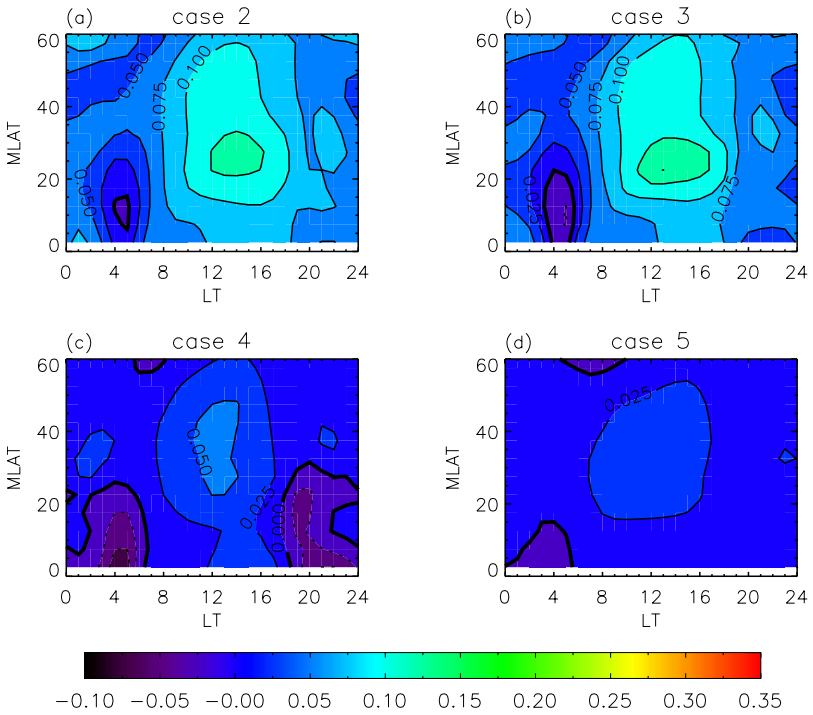

Figure 3. Local time (LT) variations of zonal mean annual asymmetry index (contour interval: 0.025) for different geomagnetic latitudes (MLAT) for five case-controlled studies using the TIEGCM (see text).

in Table 1. The simulated structures of the LT variations of zonal mean AI and the longitudinal variations of noontime AI for cases 2–5 are displayed in Figures 3 and 4.

[18] In order to test the possible influence of the geomagnetic field configuration on the annual asymmetry, we replaced the IGRF model with a tilted dipole with center coinciding with the center of the Earth in case 2, and kept other parameters the same as those used for case 1. The LT variation of the calculated zonal mean AI for different magnetic latitudes is shown in Figure 3a. The annual asymmetry in this case presents clear day-night variations, with a strong asymmetry occurring at daytime and a weak one at night. Compared to Figure 2c, the asymmetry is globally weaker. For instance, the zonal mean AI at 14 LT at 25° MLAT is about 0.2 with the IGRF field model but only 0.125 with the tilted dipole field model, and the nighttime peak is almost gone. Figure 4a gives the global structure of the AI at noon for case 2. There is a maximum of about 0.3 at 160°E and a minimum around −0.1 at 20°W at 25° MLAT. The magnitude and phase of this wave-like structure along the zonal direction vary with latitude. The secondary peak at (20°E, 20° MLAT) in Figure 2d for case 1 is absent in Figure 4a for case 2. Therefore the offset of the geomagnetic center from the geographic center has significantly impact on both the magnitude and LT variations of the zonal mean asymmetry. This offset of the poles also modifies the longitudinal pattern of the AI.

[19] In case 3, we altered the geomagnetic field configuration in the TIEGCM from a tilted dipole to a dipole field aligned with the geographic poles. The geomagnetic axis would coincide with the Earth's rotation axis. The resulting zonal mean AI in Figure 3b has almost identical amplitudes and diurnal structures as those shown in Figure 3a for case 2. However, the global AI at noon (Figure 4b) gives a longitudinal independent structure with straight contour lines along the longitude. The values of the AI are about 0.075–0.125, and the maximum lies in a zonal band between 20° and 30° MLAT. The results for case 3 suggest that the axial tilt of the geomagnetic field to the Earth's rotation axis is responsible for the main longitudinal variation of the annual asymmetry, but not for the zonal mean LT variation.

[20] Another possible cause of the annual asymmetry is the difference in the Sun-Earth distance between June and December solstices. In order to assess its effect, in case 4 we further changed the varying Sun-Earth distance to a fixed value of 1AU and keep other parameters the same as in case 3. The resulting AI LT-latitude and longitude-latitude patterns for case 4 are shown in Figures 3c and 4c, respectively. From Figure 3c, it is seen that the AI is smaller globally. Near 25° MLAT, the daytime AI is only 0.025 and the nighttime AI is basically 0.0. A peak of the AI is observed at noon near 40° MLAT and two minima (negative values) are distributed at low latitude near dawn and dusk periods. Figure 4c displays the global map of the local noon AI with typical values around 0.025–0.05. The pattern of moderate asymmetry at the latitude band between 20° and 30° shown in Figure 4b is absent in Figure 4c. A small longitudinal variation is noticed at latitude of 20–50°. It is found that the varying Sun-Earth distance accounts for about 7% asymmetry, consistent with the previous studies.

[21] Case 5 is implemented by reducing the amplitudes of migrating diurnal and semidiurnal tides by a factor of 1,000,000, consequently removing the tides. Figure 3d illustrates that the resulting zonal mean has a weak diurnal signature. The AI is still positive globally, but its magnitude

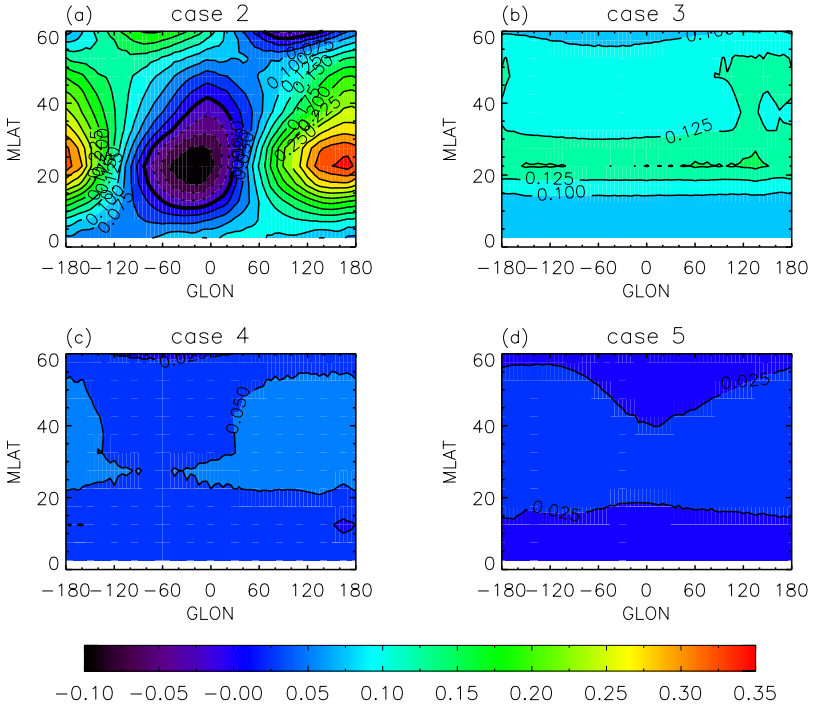

Figure 4. Global structures of midday annual asymmetry index (contour interval: 0.025) in geographic longitude (GLON) and geomagnetic latitude (MLAT) coordinates for five case-controlled studies using the TIEGCM (see text).

becomes quite small (around 0.025). Some small structures that occur in Figure 3c are not present in Figure 3d. This implies that the lower atmosphere tidal forcing modifies the annual asymmetry, but is not the primary cause of this asymmetry. Figure 4d gives the GLON/MLAT distribution of noon AI for case 5. An AI of 0.025 occurs at middle latitudes, whereas at low and high latitudes the annual asymmetry is almost gone.

4. Discussion

[22] Based on our analysis of the global asymmetry indices simulated by the TIEGCM for different cases, we can explain that the annual asymmetry is mainly driven by three factors: the geomagnetic field configuration, the Sun-Earth distance, and lower atmosphere tidal forcing.

[23] The magnetic field configuration, which can significantly influence ionospheric structures due to its strong effects on the plasma motion, is the dominant factor in producing the annual asymmetry and its variations. The tilt of the geomagnetic dipole brings on a sinusoidal variation of the field intensity and direction, as well as a variation of ionization due to the change in incident angle of solar EUV illumination over the geomagnetic equator. This consequently leads to longitudinal variations of electric fields and ion drifts by a dynamo process [*Richmond*, 1995a], and also affects the plasma transport along field lines via interaction between plasmas and the zonal neutral wind [*Walker*, 1981; *Su et al.*, 1997; *Vichare and Richmond*, 2005]. From the simulation results we conclude that the tilt of the dipole is the main cause of the longitudinal variation of the annual asymmetry at a given local time, but it does not contribute to the zonally averaged asymmetry. The offset of the geomagnetic center from the geographic center, which causes an asymmetry of the field intensity for the two hemispheres, enhances the annual asymmetry substantially at both daytime and nighttime, and results in a semidiurnal structure of the zonal mean AI. *Rishbeth and Müller-Wodarg* [2006] questioned the hemispheric asymmetry of the geomagnetic field as a major cause of the F_2-layer annual asymmetry. However, they were not able to assess how sensitive the F_2-layer asymmetry is to the variation of the magnetic field configuration using the CTIP model. In this study, we demonstrated clearly that the tilt of the geomagnetic and geographic axis is an important factor in producing the longitudinal variation of the asymmetry, which at maximum asymmetry accounts for about 40% of the asymmetry presented in case 1.

[24] The annual variation of the Sun-Earth distance, which differentiates the solar EUV radiation for different solstices, is the most obvious reason for the annual asymmetry. We investigated this factor using the TIEGCM, and found that the 3.5% discrepancy of Sun-Earth distance (i.e., 7% difference in solar radiation) between December and June solstices contributes about 0.035 to the AI on average corresponding to about 25%. This is in fair agreement with the results of *Rishbeth and Müller-Wodarg* [2006]. They investigated this factor using the CTIP model by adjusting the $F_{10.7}$ indexes for different solstices. Their study showed that solar radiation variations caused by the Sun-Earth distance differences between the two solstices enhance the annual asymmetry globally and contributes to about 0.03 to the AI on average.

[25] The migrating tides introduced at the lower boundary of the TIEGCM model propagate upward and influence the neutral winds and neutral temperatures in the ionosphere.

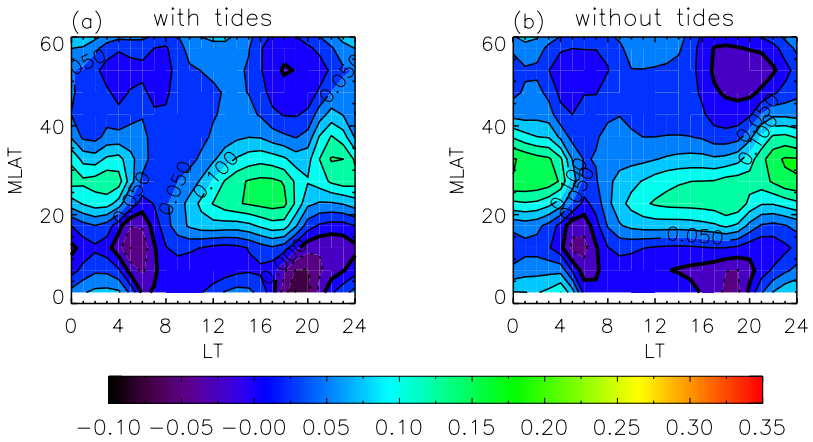

Figure 5. LT variations of the zonal mean AI for the TIEGCM simulations (a) with and (b) without tidal forcing under the IGRF geomagnetic fields and fixed Sun-Earth distances.

The variation of neutral winds causes the variation in dynamo electric fields and ion drifts. The global distribution of the ionospheric electron density is accordingly affected. Our calculations of the AI with and without tidal forcing under an aligned dipole field (cases 4 and 5) show that tidal forcing slightly enhances the annual asymmetry (Figures 3c and 3d), and also slightly adjusts the structure of the longitudinal variation of the AI (Figures 4c and 4d). The ionospheric dynamo is working through the nonlinear interaction between the neutral wind and the geomagnetic field. In order to accurately assess the tidal effects on the asymmetry, a realistic geomagnetic field model should be adopted. Two more simulations were therefore performed with (case 6) and without (case 7) tides using the IGRF field with fixed Sun-Earth distances. The LT variations of the simulated zonal mean AI for both cases are illustrated in Figure 5. Both cases have rather similar patterns of AI. The maximum asymmetries are located near 30° MLAT with two peaks around 0 LT and 16 LT. The substantial increase in the intensity of the annual asymmetry, as compared to the cases with the aligned dipole field, clearly demonstrates the significant effect of the geomagnetic configuration on the annual asymmetry. Comparison between Figures 5a and 5b also shows that the tidal forcing enhances the asymmetry on the dayside whereas it weakens the asymmetry at night. The net effect of the tides on the asymmetry is, however, not large, and is basically independent of the geomagnetic configuration used.

[26] Future work should involve investigating the detailed physical mechanisms of how the geomagnetic configuration contributes to the annual asymmetry, as well as the relationship of the annual asymmetry of the F_2-layer to variations in thermospheric composition.

5. Summary

[27] The F_2-layer annual asymmetry is an ionospheric phenomenon in which the December NmF2 is, on a global average, greater than the June NmF2. This asymmetry can only be separated from F_2-layer seasonal variations by combining data from both the northern and southern hemispheres. Thus it is difficult to obtain a global structure of the asymmetry by choosing well-matched ionosonde observations or by other ground-based observations. On the other hand, satellite observations, e.g., from COSMIC, are able to give a global picture. On the basis of nearly 1-year of COSMIC IRO observations, this study demonstrated 30% asymmetry in NmF2 globally on average. By characterizing the asymmetry with the asymmetry index, we showed that the annual asymmetry has a significant dependence on latitude, longitude and local time. A strong peak of the asymmetry occurs at about local noon and another one at midnight, both occur at 25° MLAT.

[28] Further studies were performed using the TIEGCM model. The TIEGCM simulations were able to reproduce the observed annual asymmetry and its variations to a large extent. A series of controlled case studies were made to investigate the possible physical mechanisms for the observed annual asymmetry. Our analysis of the simulation results led to the following conclusions.

[29] 1. The change in solar radiation between the December and June solstices, which is caused by the difference in Sun-Earth distances between the two solstices, contributes about 0.035 to the F_2-layer asymmetry on average, corresponding to about 7% difference (1/4 of the total asymmetry) of electron density between both solstices. During the daytime, its effect is more significant.

[30] 2. The offset of the geomagnetic center from the geographic center is the most important cause of the F_2-layer annual asymmetry and its LT variations, whereas the tilt of geomagnetic dipole is mainly responsible for the longitudinal variations of the AI. The nondipolar geomagnetic configuration would be responsible for about 45% of the asymmetry.

[31] 3. The tides from lower altitudes also contribute to the asymmetry and help to modulate the asymmetric pattern in LT. However, they are not as significant as the other two mechanisms.

[32] **Acknowledgments.** This work was supported by the Center of Integrated Space Weather Modelling (CISM), which is funded by the STC Program of NSF under agreement ATM-0120950 and a grant from the National Space Weather Program of NSF. The National Center for Atmospheric Research is sponsored by NSF.

[33] Wolfgang Baumjohann thanks Henry Rishbeth and Shunrong Zhang for their assistance in evaluating this paper.

References

Beers, T. C., K. Flynn, and K. Gebhardt (1990), Measures of location and scale for velocities in clusters of galaxies – A robust approach, *Astron. J.*, *100*(1), 32–46.

Berkner, L. V., and H. W. Wells (1938), Non-seasonal change of F2-region ion density, *Terr. Magn. Atmos. Electr.*, *43*, 15–36.

Hagan, M. E., M. D. Burrage, J. M. Forbes, J. Hackney, W. J. Randel, and X. Zhang (1999), GSWM-98: Results from migrating solar tides, *J. Geophys. Res.*, *104*(A4), 6813–6828.

Hajj, G. A., L. C. Lee, X. Pi, L. J. Romans, W. S. Schreiner, P. R. Straus, and C. Wang (2000), COSMIC GPS ionospheric sounding and space weather, *Terr. Atmos. Ocean Sci.*, *11*, 21–52.

Kelley, M. C., and R. A. Heelis (1989), *The Earth's Ionosphere: Plasma Physics and Electrodynamics*, Elsevier, New York.

Le Sager, P., and T. S. Huang (2002), Ionospheric currents and field-aligned currents generated by dynamo action in an asymmetric Earth magnetic field, *J. Geophys. Res.*, *107*(A2), 1025, doi:10.1029/2001JA000211.

Lei, J., S. Syndergaard, and A. G. Burns (2007), Comparison of COSMIC ionospheric measurements with ground-based observations and model predictions: Preliminary results, *J. Geophys. Res.*, *112*, A07308, doi:10.1029/2006JA012240.

Liu, L., B. Zhao, W. Wan, S. Venkartraman, M.-L. Zhang, and X. Yue (2007), Yearly variations of global plasma densities in the topside ionosphere at middle and low latitudes, *J. Geophys. Res.*, *112*, A07303, doi:10.1029/2007JA012283.

Manson, A., et al. (1999), Seasonal variations of the semi-diurnal and diurnal tides in the MLT: Multi-year MF radar observations from 2 to 70°N, and the GSWM tidal model, *J. Atmos. Sol. Terr. Phys.*, *61*(11), 809–828.

Mendillo, M., C.-L. Huang, X. Pi, H. Rishbeth, and R. Meier (2005), The global ionospheric asymmetry in total electron content, *J. Atmos Sol. Terr. Phys.*, *67*, 1377–1387.

Millward, G. H., I. C. F. Muller-Wodarg, A. D. Aylward, T. J. Fuller-Rowell, A. D. Richmond, and R. J. Moffett (2001), An investigation into the influence of tidal forcing on F region equatorial vertical ion drift using a global ionosphere-thermosphere model with coupled electrodynamics, *J. Geophys. Res.*, *106*(A11), 24,733–24,744.

Pancheva, D., N. J. Mitchell, and M. E. Hagan (2002), Global-scale tidal structure in the mesosphere and lower thermosphere during the PSMOS campaign of June–August 1999 and comparisons with the global-scale wave model, *J. Atmos. Sol. Terr. Phys.*, *64*, 1011–1035.

Richmond, A. D. (1995a), Ionospheric electrodynamics, in *Handbook of Atmospheric Electrodynamics,* vol. II, Hans Volland, CRC Press, Boca Raton, Fla.

Richmond, A. D. (1995b), Ionospheric electrodynamics using magnetic apex coordinates, *J. Geomagn. Geoelectr.*, *47*, 191–212.

Richmond, A. D., E. C. Ridley, and R. G. Roble (1992), A thermosphere/ionosphere general circulation model with coupled electrodynamics, *Geophys. Res. Lett.*, *19*, 601–604.

Rishbeth, H. (1998), How the thermospheric circulation affects the ionospheric F2-layer, *J. Atmos. Sol. Terr. Phys.*, *60*(14), 1385–1402.

Rishbeth, H. (2007), Thermospheric targets, *Eos Trans. AGU*, *88*(17), 189, doi:10.1029/2007EO170002.

Rishbeth, H., and I. C. F. Müller-Wodarg (2006), Why is there more ionosphere in January than in July? The annual asymmetry in the F2-layer, *Ann. Geophys.*, *24*, 3293–3311.

Sagawa, E., T. J. Immel, H. U. Frey, and S. B. Mende (2005), Longitudinal structure of the equatorial anomaly in the nighttime ionosphere observed by IMAGE/FUV, *J. Geophys. Res.*, *110*, A11302, doi:10.1029/2004JA010848.

Schreiner, W. S., S. V. Sokolovskiy, C. Rocken, and D. C. Hunt (1999), Analysis and validation of GPS/MET radio occultation data in the ionosphere, *Radio Sci.*, *34*(4), 949–966.

Schreiner, W. S., C. Rocken, S. Sokolovskiy, S. Syndergaard, and D. C. Hunt (2007), Estimates of the precision of GPS radio occultations from the COSMIC/FORMOSAT-3 mission, *Geophys. Res. Lett.*, *34*, L04808, doi:10.1029/2006GL027557.

Su, Y. Z., G. J. Bailey, K. I. Oyama, and N. Balan (1997), A model study of the longitudinal variations in the north-south asymmetries of the ionospheric equatorial anomaly, *J. Atmos. Sol. Terr. Phys.*, *59*(11), 1299–1310.

Su, Y. Z., G. J. Bailey, and K. I. Oyama (1998), Annual and seasonal variations in the low-latitude topside ionosphere, *Ann. Geophys.*, *16*, 974–985.

Vichare, G., and A. D. Richmond (2005), Simulation study of the longitudinal variation of evening vertical ionospheric drifts at the magnetic equator during equinox, *J. Geophys. Res.*, *110*, A05304, doi:10.1029/2004JA010720.

Wagner, C.-U., D. Mohlmann, K. Schafer, V. M. Mishin, and M. I. Matveev (1980), Large scale electric fields and currents and related geomagnetic variations in the quiet plasmasphere, *Space Sci. Rev.*, *26*, 391–446.

Walker, G. O. (1981), Longitudinal structure of the F-region equatorial anomaly: A review, *J. Atmos. Sol. Terr. Phys.*, *43*, 763–774.

Yonezawa, T. (1971), The solar-activity and latitudinal characteristics of the seasonal, non-seasonal and semi-annual variations in the peak electron densities of the F2-layer at noon and at midnight in middle and low latitudes, *J. Atmos. Sol. Terr. Phys.*, *33*, 887–907.

A. Burns, L. Qian, S. Solomon, and W. Wang, High Altitude Observatory, National Center for Atmospheric Research, P.O. Box 3000, Boulder, CO 80301, USA.

Y.-H. Kuo, COSMIC Project Office, University Corporation for Atmospheric Research, P.O. Box 3000, Boulder, CO 80307, USA.

J. Lei, CU/CEAS, 422 UCB, Boulder, CO 80309-0422, USA.

S. Syndergaard, Danish Meteorological Institute, Lyngbyvej 100, DK-2100, Copenhagen, Denmark.

Z. Zeng, UBC/EOS, 6339 Stores Road, Vancouver, BC, V6T 1Z4, Canada. (zzeng@eos.ubc.ca)